Stomatal opening under high temperatures is controlled by the OST1-regulated TOT3–AHA1 module

Xiangyu Xu[1,2,a], Hongyan Liu[1,2,@], Myrthe Praat[3,@,b], Gaston A. Pizzio[4], Zhang Jiang[3], Steven Michiel Driever[5], Ren Wang[1,2], Brigitte Van De Cotte[1,2], Selwyn L. Y. Villers[1,2], Kris Gevaert[6,7], Nathalie Leonhardt[8], Hilde Nelissen[1,2], Toshinori Kinoshita[9], Steffen Vanneste[1,2,10], Pedro L. Rodriguez[4], Martijn van Zanten[3], Lam Dai Vu[1,2,6,7,†,c], Ive De Smet[1,2,†,*]

[1]Department of Plant Biotechnology and Bioinformatics, Ghent University, B-9052 Ghent, Belgium
[2]VIB Center for Plant Systems Biology, B-9052 Ghent, Belgium
[3]Plant Stress Resilience, Institute of Environmental Biology, Utrecht University, Padualaan 8, 3584 CH Utrecht, The Netherlands
[4]Instituto de Biología Molecular y Celular de Plantas, Consejo Superior de Investigaciones Científicas-Universidad Politécnica de Valencia, ES-46022 Valencia, Spain
[5]Centre for Crop Systems Analysis, Wageningen University and Research, 6708 PE Wageningen, The Netherlands
[6]Department of Biomolecular Medicine, Ghent University, B-9052 Ghent, Belgium
[7]VIB Center for Medical Biotechnology, B-9052 Ghent, Belgium
[8]Aix Marseille University, CEA, CNRS UMR7265, Bioscience and Biotechnology Institute of Aix Marseille, Saint-Paul-lez-Durance, France
[9]Institute of Transformative Bio-Molecules (WPI-ITbM), Nagoya University, Chikusa Nagoya, 464-8602, Japan
[10]Department of Plants and Crops, Faculty of Bioscience Engineering, Ghent University, Ghent 9000, Belgium
[@]Equal contribution
[†]These authors jointly supervised this work
[c]Current address: Cryptobiotix SA, B-9052 Ghent, Belgium
[a]Current address: Department of Plant and Microbial Biology, University of California at Berkeley, Berkeley, CA, USA
[b]Current address: Green Biotechnology, Inholland University of Applied Sciences, Pina Bauschplein 4 1095 PN, Amsterdam, The Netherlands
[*]Corresponding author. Email: ive.desmet@psb.vib-ugent.be

Abstract

Plants continuously respond to changing environmental conditions to prevent damage and maintain optimal performance. To regulate gas exchange with the environment and to control abiotic stress relief, plants have pores in their leaf epidermis, called stomata. Multiple

environmental signals affect the opening and closing of these stomata. High temperature promotes stomatal opening (to cool down) and drought induces stomatal closing (to prevent water loss). Coinciding stress conditions, however, may evoke conflicting stomatal responses, but the cellular mechanisms to resolve these conflicts are unknown. Here, we demonstrate that the high temperature-associated kinase TARGET OF TEMPERATURE 3 (TOT3) directly controls the activity of plasma membrane H^+-ATPases to induce stomatal opening. OPEN STOMATA 1 (OST1), which regulates stomatal closure to prevent water loss during drought stress, directly inactivates TOT3 through phosphorylation. Taken together, this signalling axis harmonizes stomatal opening and closing under high temperature and/or drought. In the context of global climate change, understanding how different stress signals converge on stomatal regulation allows the development of climate change-ready crops.

Main text

Organisms are constantly subjected to a multitude of environmental and developmental cues, which collectively aim to elicit an optimal response for sustaining growth, survival, and reproduction. All organisms thus need to employ tightly controlled signalling mechanisms to optimize their response. This is particularly crucial for plants, which cannot escape from adverse conditions and are thus at the mercy of different simultaneously occurring environmental factors that strongly affect their growth, survival and performance [1–4].

Optimal leaf temperatures and water status in plants are essential for their efficient energy exchange processes [5,6]. Stomata – pores in the epidermis of plant organs – regulate the rate of gas and water vapor exchange with the environment, are entry points for pathogens, and are pivotal in shielding plants against immediate or long-term changes in environmental conditions [7–9]. Stomatal movement influences the rate of photosynthesis and respiration, thereby affecting plant water use efficiency and leaf thermal conditions [10,11]. Facing more regular concurrent high temperature and drought stress in the natural environment [12–15], plants need to initiate a range of cellular, physiological, and morphological changes to prevent damage and maintain optimal performance [1,15–17]. Opening and closing of stomata are rapid responses that likely require switch-like signalling mechanisms that can swiftly alternate when environmental conditions change. Because phosphorylation-encoded switches and oscillators within protein networks tend to be faster than genetic switches and are reversible, kinase-mediated phosphorylation relays are ideal for stomata opening and closing [18,19].

Drought stress results in dehydration and eventually wilting, and closing stomata limits water loss [8,20]. Drought-induced water deficit stimulates abscisic acid (ABA) biosynthesis and subsequently activates the ABA signalling pathway in guard cells to promote stomatal closure for plant water retention [11,21,22]. To a large part, the ABA signalling pathway regulates ion channels to control stomatal closing [23–25]. Members of the ARABIDOPSIS PM H^+-ATPase (AHA) ion pump family extrude protons from the cell and modify the membrane potential. In stomata, AHA activation drives stomatal opening [26–29]. Activation of PM H^+-ATPase activity occurs through the modification of autoinhibitory terminal domains, such as phosphorylation of the Thr947/948 residue in AHA1/2, creating a binding site for 14-3-3 proteins to release C-terminal autoinhibition [30–33]. The ABA-induced closure of stomata is largely dependent on the reduction in AHA activity, as evidenced by the insensitivity to ABA in *ost2-1D* and *ost2-2D* mutants with a constitutively active AHA1 allele [27,29,32,34]. Applying high ABA concentrations to seedlings can induce stomatal closure via attenuating AHA1 activity through Thr947 dephosphorylation [29,31,32,34,35]. OPEN STOMATA1 (OST1) is specifically expressed in guard cells and mediates stomatal closure by controlling the activity of ion transporters in response to drought through ABA-mediated pathways [36,37]. While the phosphorylation and activity of AHA are less affected in the *ost1* mutant under ABA treatment [29], it is still unclear how OST1 negatively regulates PM H^+-ATPase activity under drought conditions through ABA-mediated pathways.

In contrast, high temperature stress is accompanied by stomatal opening and enhanced stomatal conductance, resulting in a significant reduction in leaf temperature [38–41]. However, how high temperature signals are perceived and transmitted to regulate stomatal aperture is poorly understood [41,42].Upon blue-light perception, phototropins (PHOT1 and PHOT2), which also contribute to leaf cooling at high temperature [41], phosphorylate the BLUE LIGHT SIGNALLING1 (BLUS1)/MAP4K10 protein kinase. Subsequently, BLUS1 mediates phosphorylation and activation of the plasma membrane H^+-ATPase to promote stomatal opening [41,43,44]. However, the stomatal response to high temperatures also takes place in darkness, validating the involvement of additional mechanisms to regulate stomatal movement [41].

In this study, we identified and characterized a novel phosphorylation-dependent signalling axis that regulates stomatal aperture under high temperature and/or drought conditions. The high temperature-associated kinase TARGET OF TEMPERATURE 3 (TOT3)/MITOGEN-ACTIVATED PROTEIN KINASE KINASE KINASE KINASE 4 (MAP4K4) [45] directly controls the phosphorylation and activity of plasma membrane H^+-ATPases to regulate stomatal opening under high temperature. Furthermore, the regulator of ABA-mediated stomatal closure, OST1, phosphorylates and inactivates TOT3 under drought conditions to promote plant water retention. This specific phosphorylation-mediated control of TOT3 activity sheds light on the regulation of MAP4Ks and acts as a switch to mediate stomatal aperture under high temperature and/or drought conditions.

Under drought conditions, leaf temperature rises when stomata close in an ABA-dependent manner [46–48] (Supplementary Figure 1a-d). Supra-optimal air temperatures on the contrary, promote stomatal opening in the model dicot plant *Arabidopsis thaliana* and the monocot crop species *Triticum aestivum* (wheat) (Fig. 1a-d and Supplementary Figure 1e-g). This high-temperature-triggered response increases stomatal conductance and can stimulate leaf cooling through evaporation under well-hydrated conditions [40–42,49,50] *(*Fig. 1e-j and Supplementary Figure 1h-m). Based on our stomatal conductance analyses at different temperatures (Supplementary Figure 1e), we use 34°C for the majority of our assays.

Stomatal opening is partially mediated through the activation of plasma membrane H^+-ATPases, which requires phosphorylation of their penultimate threonine [27,31–33,35]. Our previous phosphoproteome analysis revealed warm temperature-mediated phosphorylation of ARABIDOPSIS H^+-ATPase 1 (AHA1) and AHA2 at their penultimate residues T948 and T947, respectively, in wild-type seedlings [45] (Supplementary Figure 2a-b). This suggests increased activity of H^+-ATPases at high temperature, which is confirmed by increased proton (H^+) release from seedlings at high temperature (Supplementary Figure 3). Indeed, *aha1* loss-of-function mutants displayed reduced stomatal aperture compared to wild-type [41] (Supplementary Figure 2c-d). Our previous phosphoproteome analyses furthermore revealed that AHA1 phosphorylation is downregulated in a loss-of-function line for the kinase TARGET OF TEMPERATURE 3 (TOT3)/MITOGEN-ACTIVATED PROTEIN KINASE KINASE KINASE KINASE 4 (MAP4K4), a conserved regulator of moderate high temperature-mediated plant growth [45] (Supplementary Figure 2e-f). Characterization of transgenic plants harbouring a transcriptional fusion between the β-glucuronidase (GUS) reporter gene and the *TOT3* promoter (*pTOT3::GUS*) indicated that, in leaves, *TOT3* is expressed in guard cells (Fig. 1k). Similarly, we detected GREEN FLUORESCENT PROTEIN (GFP):TOT3 protein in guard cells of a *tot3-2* mutant expressing *pTOT3::GFP:TOT3* (Supplementary Figure 4a). While TOT3 is phosphorylated by warm temperatures [45], *TOT3* expression was not affected by high temperature (Supplementary Figure 4b). These observations suggest a role for TOT3 in stomatal guard cells. Notably, the loss of TOT3 function does not appear to modify stomatal development (Supplementary Figure 5). These observations together suggest a role for TOT3 in controlling AHA1-mediated stomatal aperture. Indeed, we observed that not only *Arabidopsis*, but also wheat *tot3* mutants had their stomata significantly more closed at high temperature compared to their respective wild-type control lines (Fig. 1a-d and Supplementary Figure 6-8), indicating a conserved role for TOT3 in regulating dicot and monocot stomatal aperture. This role in stomatal aperture aligned with a difference in stomatal conductance of both *Arabidopsis* and wheat *tot3* mutants at high temperature, compared to wild-type control lines (Fig. 1e-j and Supplementary Figure 8-10). Furthermore, the stomatal aperture of the *Arabidopsis tot3-2* mutant at high temperature correlated with a higher leaf temperature, compared to the *tot3-2* mutant complemented with a functional GFP:TOT3 (*tot3-2 pTOT3::GFP:TOT3*) (Supplementary Figure 8 and 11).

To explore AHA1 as a potential TOT3 kinase substrate, we first confirmed that TOT3 and AHA1 proteins interact, through co-immunoprecipitation (co-IP), bimolecular fluorescence complementation (BiFC) and yeast-two hybrid (Y2H) (Fig. 2a and Supplementary Figure 12a-b). The TOT3-AHA1 interaction was unaffected by changes in temperature (Supplementary Figure 12d-f and Supplementary Table 3). Transiently co-expressing *TOT3* or *TOT3*^{D157N} (a kinase-dead version) together with *AHA1* in tobacco revealed elevated AHA1 phosphorylation at T948 in the presence of TOT3 compared to TOT3^{D157N} (Fig. 2b and Supplementary Table 1), indicating that kinase active TOT3 positively regulates AHA1 phosphorylation status. An immunohistochemical assay showed reduced phosphorylation of the penultimate AHA threonine in *tot3-2* mutant guard cells exposed to high temperature compared to *tot3-2 pTOT3::GFP:TOT3* (Fig. 2c-d and Supplementary Figure 13), supporting that AHA1 phosphorylation occurs downstream of TOT3. Subsequently, an *in vitro* kinase assay showed direct phosphorylation of the C-terminal part of AHA1 (from E905-V949, referred to as AHA1$_{905-949}$) by TOT3, which is abolished when using the non-phosphorylatable AHA1$_{905-949}^{T948A}$ variant (Fig. 2e). These results place AHA1 directly downstream of TOT3 as a substrate, to control its activity. Accordingly, the high temperature-induced increase in proton release was abolished in the *tot3-2* mutant compared to *tot3-2 pTOT3::GFP:TOT3* (Supplementary Figure 14). Finally, we uncoupled AHA1 activity from external cues or (TOT3-mediated) phosphorylation of the penultimate T948 both genetically through testing *open stomata2-2D* (*ost2-2D*), an *aha1* allele with constitutively activated H^+-ATPase activity [27], and pharmacologically through using fusicoccin, an activator of plasma membrane H^+-ATPases [27,31,35,51]. Introducing *ost2-2D* in *tot3-2* and treating *tot3-2* with fusicoccin both rescued the stomatal aperture phenotype of *tot3-2* at high temperature (Fig. 2f-g and Supplementary Figure 15). Taken together, we show that TOT3 regulates stomatal aperture through controlling AHA1 activity by direct phosphorylation of T948.

AHA activity is down-regulated by a SnRK2-dependent ABA pathway to induce stomatal closure [29,34,37]. To investigate whether TOT3 activity is also mediated by ABA, we performed an *in vitro* kinase assay using TOT3 isolated from *Arabidopsis* plants. High temperature promotes TOT3 activity; but, in the presence of ABA or drought, which elevates ABA levels [52,53], high temperature-activated TOT3 autophosphorylation was reduced (Supplementary Figure 16). These data imply that ABA and drought modulate TOT3 activity and subsequently AHA1-mediated stomatal movement. OPEN STOMATA 1 (OST1)/SnRK2.6, is specifically expressed in guard cells [36,37] (Supplementary Figure 17) and is involved in ABA-mediated stomatal closure under drought stress. Hence, the *ost1* loss-of-function mutant exhibits constitutively open stomata and consequently cooler leaves [36,37,54] (Supplementary Figure 18), which contrasts with the *tot3* phenotype (Fig. 1a-b and Supplementary Figure 6). The partial reversion of the *ost1-3* constitutively open stomata phenotype in *tot3-2 ost1-3* double mutants (Supplementary Figure 19), is consistent with TOT3 and OST1 acting in the same pathway. We next showed that TOT3 and OST1 co-localize in stomata and interact (Fig. 3a and Supplementary Figure17 and 20). This interaction was not dependent on, nor affected by, ABA or high temperature [55] (Supplementary Figure 20). Our genetic and biochemical data confirm previous results where TOT3 was listed as an OST1-INTERACTING PROTEIN [55], and indicate that TOT3 and OST1 could function together during high temperature and/or drought signalling at the level of stomatal aperture control.

We next tested whether TOT3 could be phosphorylated by ABA-activated OST1. Indeed, mass spectrometry analyses revealed several TOT3 phosphosites that were up-regulated *in planta* by ABA and/or OST1 compared to control conditions (Fig. 3b-c and Supplementary Figure 21, Supplementary Table 2). Since some ABA-responsive TOT3 phosphosites, such as S324 or S481, were not directly regulated by OST1 (Supplementary Figure 22), we focused on those TOT3 phosphosites that were regulated by ABA-activated OST1: S382, S448 and S451

(Fig. 3b-c). For the functional analyses of the phosphorylated serines, we either used Glu substitutions as a mimetic for serine phosphorylation or we used Ala substitutions of these residues together with 2 neighboring residues that might otherwise compensate for the loss of phosphorylation. An *in vitro* kinase assay using an *E. coli*-expressed *TOT3* fragment encompassing those phosphosites (GST:TOT3$_{365\text{-}465}$) and His:MBP:OST1 confirmed that OST1 directly phosphorylates TOT3 (Fig. 3d). In contrast, a TOT3 phosphomutant variant where these sites, together with two additional adjacent serine residues (S381 and S383; generating GST:TOT3$_{365\text{-}465}^{S381A/S382A/S383A/S448A/S451A}$, here referred to as GST:TOT3$_{365\text{-}465}$-5A) were mutated, exhibited largely reduced OST1-mediated phosphorylation (Fig. 3d), indicating that direct OST1 phosphorylation target site(s) is/are among these residues.

To assess if OST1-mediated phosphorylation of TOT3 affected TOT3 function, we tested the phosphomutant GFP:TOT3-5A and phosphomimetic (GFP:TOT3$^{S382E/S448E/S451E}$, here referred to as GFP:TOT3-3E) proteins for their ability to rescue the *tot3-2* stomatal aperture phenotype at high temperature. Three independent *tot3-2 pTOT3::GFP:TOT3-3E* lines could not rescue the *tot3-2* stomatal aperture phenotype, while three independent *tot3-2 pTOT3::GFP:TOT3-5A* lines did rescue the *tot3-2* stomatal aperture phenotype (Fig. 3e and Supplementary Figure 23). Moreover, expression of *GFP:TOT3-3E* did not alter the partial rescue of the *ost1-3* stomata aperture phenotype by the *tot3-2* allele (Supplementary Figure 24). Taken together, this suggests that OST1-mediated phosphorylation of TOT3 leads to a less functional TOT3 protein. Notwithstanding lines expressing *TOT3-3E* also exhibited reduced TOT3 protein levels (Supplementary Figure 23), we assessed if TOT3-3E was unable to – in part – rescue the *tot3-2* mutant due to altered kinase activity through *in vitro* kinase assays. This indeed revealed reduced kinase activity for TOT3-3E, considering autophosphorylation and AHA1 phosphorylation, while TOT3-5A showed increased kinase activity, compared to an equal amount of TOT3 protein (Fig. 3f). Consistently, transient expression of *TOT3-5A* or *TOT3-3E* in *N. benthamiana* leaves resulted in similar TOT3 protein levels, but an increased (*TOT3-5A*) or decreased (*TOT3-3E*) phosphorylation of AHAs (Supplementary Figure 25a). The phosphorylation levels of AHA1-T948 and AHA2-T947 were significantly increased in *tot3-2 pTOT3:GFP:TOT3-5A #1* (Supplementary Figure 25b). This aligned with an increased proton release in *tot3-2 pTOT3:GFP:TOT3-5A* under control temperature (Supplementary Figure 25c), indicating increased TOT3-5A activity independent of high temperature-mediated activation. These results support that TOT3-5A is hyper-active and TOT3-3E is inactive, and thus that OST1-mediated phosphorylation of TOT3 at positions S382, S448, and S451 predominantly leads to a less active TOT3 protein. However, we cannot fully exclude an additional effect on TOT3 protein abundance.

We next tested if OST1-mediated regulation of TOT3 activity is indeed functionally relevant under drought and/or high temperature stress in *Arabidopsis* seedlings. We first observed reduced phosphorylation of TOT3-S448 at high temperature, which was independent of OST1, and increased phosphorylation upon both ABA treatment (Fig. 4a and Supplementary Figure 26-27, Supplementary Table 3) and drought stress (Fig. 4b and Supplementary Table 4). Furthermore, drought-regulated TOT3-S448 phosphorylation depended on OST1 (Fig. 4c), while OST1 was not required for high temperature-increased TOT3 activity (Fig. 4d). These results indicate that under drought stress and under high ABA levels, where stomatal closure occurs, phosphorylation of TOT3 on OST1-target residues occurs, to inactivate TOT3. Indeed, *tot3-2 pTOT3:GFP:TOT3-5A* lines were less sensitive to ABA with respect to a reduction of stomatal aperture (Fig. 4e). These results support that specific OST1-mediated phosphorylation controls TOT3 activity under drought stress conditions. Furthermore, the *tot3-2* mutant and *tot3-2* expressing *GFP:TOT3-3E* were more tolerant to progressive drought stress than *tot3-2* expressing *GFP:TOT3* or *GFP:TOT3-5A* (Fig. 4f-g), suggesting that TOT3 activity contributes to drought responsiveness and resilience.

Our results support that opposite regulation of stomatal opening under high temperature and during drought stress correlates with TOT3 activity. This suggests that these conflicting stress conditions converge on TOT3 activity to achieve an integrated response. The opposing effect of both stress conditions on TOT3 activity and stomatal aperture highlights an apparent signalling conflict during combined high temperature and drought stress. To reveal the hierarchy of TOT3 signalling, we exposed a line with increased OST1-independent TOT3 kinase activity (*pTOT3::GFP:TOT3-5A* in *tot3-2*) to the combination of drought and increased temperature. This revealed that preventing TOT3 inactivation leads to cooler leaves under these combined stresses, compared to the *tot3-2 pTOT3::GFP:TOT3* control line and compared to exposure to the individual stresses (Fig. 4h and Supplementary Figure 28). This implies that drought-induced, OST1-mediated inactivation of TOT3 is essential to close stomata under drought conditions if, at the same time, a high-temperature signal pushes to keep these open.

Plants can be simultaneously exposed to different environmental stresses, such as high temperature and drought, and require ongoing adjustments to optimize their growth, performance, and survival. Recent studies have increased our understanding of thermomorphogenesis, exhibiting how plants possess phenotypic plasticity, adjusting their morphology and growth in response to temperature stimuli [56]. The development and movement of stomata also play a pivotal role in supporting plant growth and survival amidst challenging and dynamic elevated temperature environments [40,41]. A pivotal question that remains unanswered is how guard cells efficiently integrate signals to optimize stomatal opening [42]. Stomatal opening facilitates plant growth through increased carbon dioxide absorption and transpiration, both vital for photosynthesis and nutrient uptake from the soil [6,57]. Additionally, this opening aids in cooling leaf temperatures during high temperature stress, maintaining favourable cellular conditions for metabolism [6,57]. A recent study revealed that elevated temperatures influence guard cell movement through phototropins and plasma membrane (PM) H^+-ATPase activity [41]. The membrane-associated kinase TOT3 regulates thermomorphogenesis, independently of the crucial warm temperature response regulators phytochrome B (phyB) and PHYTOCHROME-INTERACTING FACTOR 4 (PIF4) [45]. Here, we demonstrated that TOT3 is also required for stomatal movement in Arabidopsis and wheat under high temperatures, and specifically that TOT3 directly phosphorylates AHA1 and positively regulates H^+-ATPase activation in the guard cells to promote stomatal opening and leaf cooling in Arabidopsis (Fig. 4i). This insight bridges a gap in our comprehension of how plants facing elevated temperatures manage leaf temperature via stomatal regulation. In addition, our results add another kinase to the growing list of kinases that (in)directly affect the phosphorylation of AHAs, such as BLUS1, TRANSMEMBRANE KINASE1 (TMK1), and FERONIA (FER) [41,51,58,59]. On the other hand, stomatal opening can result in excessive water loss from plants under drought conditions, in which ABA synthesis is triggered to initiate stomatal closure to mitigate water loss [21,60,61]. Our findings also establish a connection where ABA-activated OST1 directly phosphorylates and inactivates TOT3 and/or leads to reduced TOT3 levels to regulate H^+-ATPase activity under drought stress (Fig. 4i and Supplementary Figure 23). Furthermore, TOT3 kinase activity is enhanced under high temperature, but the high temperature-induced TOT3 activity is repressed under combined high temperature and drought treatment. This accelerate-and-brake mechanism allows fast and flexible harmonization of conflicting signals arising from high temperature and drought cues to optimize the stomatal aperture to effectively deal with multiple stresses. It should be noted that some of our results are based on transient expression of key proteins in *N. benthamiana* and the results might not fully reflect the situation in *Arabidopsis*. Unexpectedly, we also observed a high temperature-induced increase in OST1 activity (Supplementary Figure 29), suggesting additional layers of complexity within the OST1-TOT3-AHA1 signalling module under high temperature. These

insights increase our understanding of how different environmental signals are interpreted to fine-tune plant responses, which provides opportunities for crop resilience improvement.

Methods

Plant materials and growth conditions

All *A. thaliana* mutants and transgenic lines used in this study are in the Col-0 genetic background, unless otherwise indicated. TOT3 (AT5G14720), OST1 (AT4G33950), AHA1 (AT2G18960) and AHA2 (AT4G30190) are the main factors studied in this paper. The following *A. thaliana* lines were used: *tot3-1 (SALK_065417)* [45], *tot3-2 (SALK_086087)* [45], *ost1-3 (SALK_008068)* [54,62] and *ost1 (SALK_067550C)* [62]. Lines were ordered from the Eurasian *Arabidopsis* Stock Centre (NASC). The *aha1-6*, *aha1-8*, *ost2-2D* mutant and *tot3-2* complementation line *tot3-2 pTOT3::GFP:TOT3 #5 and #7 (TOT3 tot3-2 #5 and TOT3 tot3-2 #7)* have been described previously [27,41,45]. The TOT3 phosphomutant *tot3-2 pTOT3::GFP:TOT3 S381A/S382A/S383A/S448A/S451A (TOT3-5A tot3-2)* and phosphomimetic *tot3-2 pTOT3::GFP:TOT3 S382E/S448E/S451E* (*TOT3-3E tot3-2)* are generated in this study (see below and Supplementary Table 6). *Arabidopsis* seeds were sterilized with 70% ethanol and sown on half Murashige and Skoog (MS) growth medium containing 1% sucrose (per litre: 2.15 g of MS salts, 0.1 g of myo-inositol, 0.5 g of MES, 10 g of sucrose and 8 g of plant tissue culture agar; pH 5.7). Seeds were stratified at 4°C for 2 days in the dark and then moved to 21°C under continuous light for germination for 48 h. Afterwards, seedlings were grown at 21°C under 70% ± 10% relative humidity under long-day conditions (16 h light/ 8 h darkness) (unless indicated otherwise). All *Triticum aestivum* plants in this study are in the Cadenza accession genetic background. Wheat TOT3 homologue (TraesCS7D01G232400) mutants Cadenza 1716 (*tot3* W122*) and Cadenza0256 (*tot3* Q191*) have been described previously [45]. Wild-type lines were selected from the backcrossing with the respective Cadenza TILLING line. The seeds were put on wet paper enclosed by plastic wrap for two days at 4 °C. After stratification, the seeds were transferred to 21°C in darkness for 2 days to allow germination. Seeds that germinated uniformly were selected and grown in plastic pots containing Jiffy 7c pellets (Jiffy Products International AS, Norway) under 21°C with 70% ± 10% RH condition and 16h light/8h dark, 90 µmol m^{-2} s^{-1} photosynthetically active radiation cool-white (fluorescent tungsten tubes, Osram). Unless indicated otherwise, we conducted our experiments under controlled humidity or VPD conditions under well-watered conditions (in soil) (Supplementary Figure 1m and Supplementary Figure 10) or closed plates (Extended Data Fig 1l), ensuring the absolute absence of environmental drought stress. Unless otherwise mentioned, plants of the indicated age were exposed to 21°C or 34°C for 2 hours to assess stomatal aperture. Detailed information on the growth conditions for high temperature experiments, drought experiments, and stomatal conductance analyses can be found in the Extended Methods in the Supplementary Information.

Plasmid constructs and generation transgenic lines

PCRs were performed by Q5® High-Fidelity polymerase according to the manufacturer's instructions (New England Biolabs, USA) with primer pairs (Supplementary Table 5). The CDS of TOT3-3E and TOT3-5A were synthesized (Twist Bioscience, USA). For the various plasmids, the construct information and cloning system are provided (Supplementary Table 6). The GoldenGate cloning system, Gateway cloning system, Gibson assembly and restriction cloning were used to generate the plasmids according to the associated protocols (Supplementary Table 6). Plasmids were checked by PCR and sequenced with suitable primers (Supplementary Table 5). Plant vectors were transformed in *Agrobacterium tumefaciens* C58C1 and plant transformation was performed using the floral dip method as previously described [63].

Leaf temperature under abscisic acid (ABA) treatment
The experiments were performed with soil-grown Col-0 plants (10 leaf stage) at 21°C sprayed with 10 µM ABA (10 mM ABA stock dissolved in EtOH and diluted in 0.025% (v/v) Silwet or Mock (0.025% (v/v) Silwet with identical volume of EtOH). Thermal images were taken every 15 min during the photoperiod continuously using FLIR ResearchIR Max software (version 4, FLIR Inc., USA).

Thermal imaging and leaf temperature quantification
Thermal images of plants on plates were captured using a PI 200 infrared thermography camera, (Germany) from the top of the plants from a fixed distance. All genotypes in each plate were recorded together. Leaf temperature quantification was processed in optris PIX Connect (version 2.18.2239.0, Germany). The middle region of each leaf of one plant was measured to get the average leaf temperature of each plant. Thermal images of plants on soil were recorded by a FLIR A655sc High Resolution LWIR thermal imaging (IR) camera (Teledyne FLIR LLC, USA) using FLIR ResearchIR Max software (version 4, USA). Acquired thermal images were analyzed using ImageJ software. To measure the leaf temperature of each plant a region of interest was drawn on one mature leaf per plant and measurements were taken every 4th hour, at ZT = 0, 4, and 8 h (8h photoperiod) and ZT = 12, 16, 20 (16 h darkness period), throughout the experimental period. For every 6th image (i.e., equaling every 24 h), the measured region of interest was manually adjusted for each leaf per plant to correct for leaf growth and movement, assuring that the same region of each leaf was measured throughout the experimental period.

Stomatal aperture assay with fusicoccin treatment
Stomatal aperture assays were performed as previously described [41]. Three-week-old plants grown on Petri plates under long-day conditions at 21°C were used. Mature leaves were incubated overnight in a buffer containing 10 mM MES-KOH and 50 mM KCl, pH 6.15 at 21°C in the dark to induce stomatal closure. Subsequently, leaves were transferred to the same buffer containing 10 µM fusicoccin dissolved in DMSO or 0.1% DMSO (mock) as the negative control. The leaves were incubated at 21°C or 34°C for 2 h before imaging with Zeiss 710 inverted confocal microscope. The images were used for stomatal aperture measurement.

Stomatal aperture assay with abscisic acid (ABA) treatment
The experiments were performed with plants grown on half-strength MS medium petri plates covered with sterilized nylon mesh (PROSEP, Belgium). Seeds of different genotypes were sown of divided parts of plates in replicates to avoid position effects. After 2 days of stratification at 4°C, the plates were kept in long-day conditions (16h light/8h dark, 90 µmol m^{-2} s^{-1} photosynthetically active radiation and 70% RH) for 3 weeks at 21 °C. After 3 weeks, the mesh with growing plants was transferred to half MS plates with 10 µM ABA or DMSO (mock) and treated for another 2 hours at the above condition. The 3rd leaf was used for leaf imprinting.

Leaf imprint and stomatal quantification
To detect stomatal aperture from intact plants, leaf imprint assays were performed with modifications as described [64–66]. After 2h exposure to 21°C or 34°C, the 3rd true leaf of 3-week-old *Arabidopsis* or wheat plants was used for taking the imprint. Moderate pressure was used to mix the catalyst and polysiloxane (3M™ ESPE Express light body, USA). The mixture was applied to the abaxial surface of the leaf using toothpicks with minimal pressure. After the mixture was hardened, the leaf imprint was separated from the leaf. Transparent nail varnish was covered on the hardened imprints and dried to make a positive imprint. Scanning electron microscope (SEM) TM1000 (Hitachi, Japan) was used to scan the leaf center part of the positive

imprints (Supplementary Figure 5a). The obtained images were measured and quantified using ImageJ software (version 1.53f). The aperture of normal-looking, well-imaged stomata was calculated as a ratio by the length divided by the width of the aperture.

Observation of stomatal aperture using Arabidopsis leaf epidermal peels

To observe the stomatal aperture, the epidermal peel preparation and stomatal movement observation were performed as described, with some modifications [67,68]. Briefly, the 3rd true leaf of 3 to 4-week-old *Arabidopsis* grown on 1/2 MS medium were detached and abaxial peels were separated. Isolated peels were incubated in stomata reaction buffer (10 mM MES-KOH, 50 mM KCl, 0.1 mM $CaCl_2$, adjusted to pH 6.5 with 1 M KOH). After a 2-hour incubation in the dark at 21°C to synchronize stomatal closing, the peels were transferred to 34°C in darkness for 2 hours. The peels were then immediately imaged using an Olympus BX51 microscope following the indicated treatment.

Quantitative analysis of stomatal density and index

The stomatal density and index measurement and analysis were performed as described [69]. Detailed information can be found in the Extended Methods in the Supplementary Information.

Histochemical β-Glucuronidase (GUS) Staining

Two-week-old plants grown under continuous light were used for GUS staining. Plants were fixated in cold 90% (v/v) acetone until the leaves turned white. Leaves were rinsed with NT buffer (100 mM Tris/50 mM NaCl). After that, the samples were incubated in NT buffer containing 2 mM K3[Fe(CN)6] and 2 mM X-Gluc for staining at 37°C for 2h. The plants were rinsed with NT buffer to remove the staining agents and mounted on glass slides in 80% (v/v) lactic acid. The images were taken using an Olympus BX53 (Olympus, Japan).

Determination of plant proton release under high temperature

The assay was performed as described [70,71]. Briefly, seeds were germinated and grown on vertical half MS petri plates for 7 days. Seedlings were transferred to a flask (5 seedlings/flask) and washed with assay solution (one-quarter strength MS and 2 mM MES buffer, pH 6.8) for 5 min. In each flask, 6 mL of half MS liquid medium was added, and the seedlings were allowed to grow for 2 weeks. Acidification assays were then performed in fresh assay solution under indicated temperatures while shaking in the growth chamber (TC 445S, Tintometer GmbH) set at identical environmental conditions (70% RH and 90 µmol m^{-2} s^{-1} PAR) for 8 hours. H^+ release was calculated by taking the difference between the initial and final pH and normalized to the total fresh weight of the plants.

Immunohistochemical detection of AHA and the phosphorylation of the AHA penultimate residue in guard cells

Immunohistochemical detection was performed according to a previously published method by using an immune-robot; InsituPro Vsi II (Intavis) [29,72]. A detailed description can be found in the Extended Methods in the Supplementary Information. The fluorescence signal of guard cells was captured by a Leica SP8 confocal microscope (Leica, Germany) and gating technology was applied for autofluorescence removal. The fluorescence intensities of stomata were quantified using ImageJ (version 1.53f), for which each stomate was circled, and the average intensity of the area was calculated as previously described [29,73,74].

Tobacco infiltration

Agrobacterium tumefaciens strain C58 was transformed with the indicated plasmids (Supplementary Table 6). Five- to six-week-old *Nicotiana benthamiana* leaves were infiltrated

as previously described [45].

Bimolecular fluorescence complementation and quantification.
The BiFC method was modified based on the previously described protocol [75]. A detailed description can be found in the Extended Methods in the Supplementary Information. The obtained images were measured using ImageJ (version 1.53f) as described [76]. The separate images with the YFP channel or RFP channel were exported to ImageJ and the average signal of each channel on the whole image was calculated. The ratio of YFP/RFP was calculated.

Protein extraction, co-immunoprecipitation, and Western blot
Plant materials were collected and ground in liquid nitrogen with a mortar and pestle until they became fine powder. Total proteins were extracted as previously described [45]. A detailed description can be found in the Extended Methods in the Supplementary Information.

Recombinant protein purification
The plasmids (Supplementary Table 6) were transformed into *E. coli* strain BL21 (DE3). The protein purification method was modified based on the previously described [45]. Detailed information can be found in the Extended Methods in the Supplementary Information.

Co-immunoprecipitation of recombinant proteins
One μg recombinant GST or GST-OST1 protein was mixed with 50 μL Glutathione Sepharose 4B beads in 1 mL PBS buffer at 4°C for 2 h with rotation. After that, the supernatant was removed by centrifugation. One μg MBP-TOT3-His recombinant proteins was added onto GST- or GST-OST1-bound beads and incubated at 4°C for 2 h with rotation. The supernatant was separated from the beads by centrifugation and removed. Beads were washed 5 times with 1 mL PBS each. Proteins were separated by SDS-PAGE and S-gel and Western Blot was performed as described above using anti-His at 1:2000 dilution (Qiagen, Germany) as the primary antibody and anti-mouse antibody at 1:10000 dilution (Cytiva, USA) as the secondary antibody.

Radioactive kinase assay for recombinant proteins
Three μg of purified substrate protein and one μg purified kinase were incubated at 30°C for 1 h in kinase assay buffer (10 mM Tris-HCl pH 7.5, 2 mM $MnCl_2$, 10 mM $MgCl_2$, 0.5 mM DTT, 5 μM ATP and 5 μCi [γ-32P]ATP) in a total volume of 30 μL. The kinase reaction was stopped by adding Laemmli sample buffer and Sample Reducing Agent and incubation for 10 min under 70°C. Proteins were separated by SDS–PAGE. Phosphorylation was visualized by autoradiography. Coomassie staining was performed as the loading control.

Radioactive kinase assay for planta immunoprecipitated proteins
For western blots or kinase assays using the proteins extracted from plants, 2-week-old *tot3-2 pTOT3::GFP:TOT3* plants that were grown at 21°C under continuous light were used. Plants were firstly moved to a half-strength MS petri plate with 50 μM ABA or DMSO at 21°C for 2 h and then the plates were transferred to 21 or 34°C for another 2 h. Leaves were collected and ground into powder for protein extraction and co-immunoprecipitation with GFP or RFP magnetic beads as described above. After immunoprecipitation and washing, the beads were resuspended in kinase assay buffer as described above and incubated at 30°C for 1 h. The kinase reaction was stopped by adding Laemmli sample buffer and Sample Reducing Agent and incubation for 10 min at 70°C. Proteins were separated by SDS–PAGE. Phosphorylation signals were detected by autoradiography. Silver staining or Coomassie staining was performed as the loading control. The phosphorylation intensity of the target protein in autoradiographs was

measured using ImageJ (version 1.53f). The protein amount was measured to normalize phosphorylation intensity. The mock condition was set to 1 as the basal level to calculate the relative phosphorylation level for the treatments.

Radioactive kinase assay of TOT3 under combined high temperature and drought treatment
The radioactive kinase assay was performed as described previously with adaptations [77]. A detailed description on plant growth conditions and radioactive kinase assay can be found in the Extended Methods in the Supplementary Information.

Yeast two-hybrid assay
To test for interaction between TOT3 and OST1, the yeast strain AH109 was co-transformed with *pBRIDGE-OST1* and *pGADT7-TOT3* and the corresponding controls with an empty vector. Co-transformed yeast colonies were selected in a liquid synthetic defined (SD) medium lacking Leu and Trp, and two independent colonies were grown for interaction assays. A Y2H growth assay determined the interaction on medium lacking Leu, Trp and His. Dilutions (10^{-1}, 10^{-2}, 10^{-3}) of saturated cultures were spotted onto the plates and photographs were taken after 5 days at 30ºC. For the interaction of TOT3 and AHA1, the assay was performed as described before [78]. NubG-TOT3 with AHA1-Cub-PLV and the corresponding controls were transformed into Yeast strain THY.AP 4 [*MATa ura3 leu2 lexA::lacZ::trp1 lexA::HIS3 lexA::ADE2*]. Co-transformed yeast colonies were selected in a liquid synthetic defined (SD) medium lacking Leu and Trp, and followed by selection on SD medium lacking Leu, Trp, His and Ade. Dilutions (10^{-1}, 10^{-2}, 10^{-3}) of saturated cultures were spotted onto the plates and photographs were taken after 3 days at 30ºC.

RT-qPCR
Two-week-old *Arabidopsis* seedlings were grown at 21°C under continuous light and transferred to 34°C or kept at 21°C for 2 h. The shoot of the seedlings was harvested for detection of gene expression. At least three biological replicates were performed for each experiment. RNA Tissue Miniprep (Promega, USA) was used for RNA extraction and purification under the manufacturer's instruction. cDNA synthesis was performed from 1 µg RNA with qScript cDNA Synthesis Kit (Quantabio, USA). qRT-PCR was performed with primers provided in (Supplementary Table 5) on a LightCycler 480 (Roche Diagnostics) with LightCycler 480 SYBR Green I Master (Roche) according to the manufacturer's instructions.

Mass spectrometry (MS) analysis of proteins expressed in tobacco leaves
The assay was performed as described[79]. Briefly, two separate experiments were performed. In the first experiment, plasmids containing *35S::GFP:TOT3* and *35S::RFP:OST1* (Supplementary Table 6) were co-infiltrated in tobacco leaves. After 3 days, the leaves were infiltrated with 50 µM ABA or DMSO for 2 h and then collected. In the second experiment, plasmids containing *35S::GFP:TOT3* or its mutated variants $TOT3^{D157N}$ [45], *TOT3-3E* and *TOT-5A* (Supplementary Table 6) were co-infiltrated with *35S::RFP:AHA1*. The samples were harvested after 3 days. For all experiments, four biological replicates were performed. Immunoprecipitation of GFP-TOT3 (for the first experiment) or RFP-AHA1 (for the second experiment) was performed, and LC-MS/MS analyses were carried out as previously described to detect the phosphorylation of the immunoprecipitated proteins [45]. Peptide searches were performed using Maxquant software (version 1.6.10.43) on the UseGalaxy.be server. A database containing all *Nicotiana benthamiana* protein sequences from SolGenomics and the protein sequences of GFP, RFP, GFP-TOT3 and RFP-OST1 (for the first experiment) or GFP, RFP, GFP-TOT3 and RFP-AHA1 (for the second experiment) were used as the search database. All phosphosites with at least 3 valid values in one treatment group were retained as reproducibly

quantified phosphosites for statistical analysis. Multiple sample test or unpaired t-test with $p < 0.05$ was carried out to test the differences among the treatments.

Immunoprecipitation-Mass Spectrometry

Two-week-old *tot3-2 pTOT3::GFP:TOT3 #5* seedlings grown on square petri plates with half-strength MS under long-day conditions (16 h light/8 h dark, 90 µmol m^{-2} s^{-1} photosynthetically active radiation and 70% relative humidity (RH)) were used. Whole seedlings were moved to flasks with liquid half-strength MS, containing DMSO (mock) or 50 µM ABA (ABA) at 21°C, or DMSO at 34°C (high temperature) under identical light and humidity conditions for 1 h (see Supplementary Figure 1d for the conditions). The shoot of the seedings was collected. Protein extraction and GFP-immunoprecipitation were performed as described above (***Mass spectrometry (MS) analysis of proteins expressed in tobacco leaves***). Peptide searches were performed using Maxquant software (version 1.6.17.0) on the UseGalaxy.be server. A database (Araport11_genes.201606.pep) containing *Arabidopsis thaliana* protein sequences and the protein sequences of GFP-TOT3 was used as the search database. All phosphosites with at least 3 valid values in one treatment group were retained as reproducibly quantified phosphosites for statistical analysis. Multiple sample test with $p < 0.05$ was carried out to test the differences among the different treatments.

Phosphopeptide enrichment and LC-MS/MS analysis

Phosphoproteome analyses on plants under drought conditions were performed as described above (see ***Drought experiments*** for experimental set-ups). Protein extraction and phosphoproteomics were performed as previously described [45]. A detailed description can be found in the Extended Methods in the Supplementary Information. MS/MS spectra were searched against the Araport11 database for *Arabidopsis thaliana* (Araport11_genes.201606.pep) by the MaxQuant software (version 1.6.17.0). The 'Phospho(STY).txt' output file generated by the MaxQuant search was loaded into Perseus software (version 1.6.7) for analysis. All data were selected first by a localization probability cut-off of > 0.75. Phosphosites quantified in at least three out of biological replicates for at least one genotype under one condition were retained. Log2 phosphosite intensities were centred by subtracting the median of the entire set of protein ratios per sample. Imputation was subsequently processed with default values for "Width = 0.3" and "Down shift = 1.8" by the mode of separately for each column [80]. Differential TOT3 phosphosites were selected in Perseus based on the two-sample test ($p < 0.05$) between (i) well-watered and drought in Col-0 wild-type and (ii) Col-0 and *ost1-3* under drought conditions.

Experimental control, quantification and statistical analyses

The majority of the experiments were randomized, and relevant analyses were performed mainly blinded with respect to sample identity during experiments and outcome assessment. The quantification of BiFC, stomatal assays and guard cell H^+-ATPase immunohistochemical detection were done in a blinded set-up involving several co-authors either labelling or measuring the samples/images. Most experiments were repeated two to three times and all biological replicates gave similar results. Statistical analyses were performed in GraphPad Prism (version 9.5.1).

Statistics and Reproducibility

All *p* values were calculated in GraphPad Prism (version 9.5.1) using a t-test, a one-way ANOVA or a two-way ANOVA, and all the calculated *p*-values and associated statistical outputs are added in the Source Data. No statistical methods were used to predetermine sample

size. Investigators were not blinded to allocation during experiments and outcome assessment. Experiments were repeated with indicated times in each figure legend. All attempts at replication were successful.

Data availability

Data are available in the Supplementary materials, including the source data. Mass spectrometry proteomics data are available via ProteomeXchange with identifier PXD044300.

Acknowledgements

We thank Daniel Van Damme and Bert De Rybel for critical comments on the manuscript. We thank Edward Farmer for providing *ost2-2D* seeds, Michael Broberg Palmgren for *aha1-6* seeds, and the Eurasian Arabidopsis Stock Centre for providing various seeds. This work was supported by MCIN/AEI/ 10.13039/501100011033 grant PID2020-113100RB) (to PLR), Graduate School Green Top Sectors grant GSGT.2018.007 of the Netherlands Organization for Scientific Research (NWO) (to MP and MvZ), UGent BOF postdoctoral mandate 01P12219 (to LDV), UGent BOF doctoral mandate 01CD7122 (to XX), China Scholarship Council grant 201708340063 (to RW), China Scholarship Council grant 201706350153 (to XX), China Scholarship Council grant 201806170025 (to JZ), and China Scholarship Council grant 202204910025 (to HL).

Author Contributions Statement

Conceptualization: IDS, LDV; Funding acquisition: PLR, MP, MvZ, LDV, ZJ, XX; Investigation: XX, HL, LDV, MP, NL, BVDC, GAP, ZJ, RW, SMD, SLYV; Supervision: IDS, LDV, KG, MvZ, PLR, HN, SV; Tools: TK; Visualization: XX, LDV, IDS; Writing – original draft: XX, IDS, LDV; Writing – review & editing: XX, MP, ZJ, KG, NL, PLR, MvZ, SMD, SV, HN, LDV, IDS.

Competing Interests Statement

The authors declare no competing interests.

References

1. Zhang, H., Zhu, J., Gong, Z. & Zhu, J.-K. Abiotic stress responses in plants. *Nat. Rev. Genet.* **23**, 104–119 (2022).
2. Zhu, J. K. Abiotic Stress Signaling and Responses in Plants. *Cell* **167**, 313–324 (2016).
3. Waadt, R. *et al.* Plant hormone regulation of abiotic stress responses. *Nat. Rev. Mol. Cell Biol.* **23**, 680–694 (2022).
4. Kollist, H. *et al.* Rapid Responses to Abiotic Stress: Priming the Landscape for the Signal Transduction Network. *Trends Plant Sci.* **24**, 25–37 (2019).
5. Gampe, D. *et al.* Increasing impact of warm droughts on northern ecosystem productivity over recent decades. *Nat. Clim. Chang.* **11**, 772–779 (2021).
6. Dusenge, M. E., Duarte, A. G. & Way, D. A. Plant carbon metabolism and climate change: elevated CO 2 and temperature impacts on photosynthesis, photorespiration and respiration. *New Phytol.* **221**, 32–49 (2019).
7. Murata, Y., Mori, I. C. & Munemasa, S. Diverse Stomatal Signaling and the Signal Integration Mechanism. *Annu. Rev. Plant Biol.* **66**, 369–392 (2015).
8. Hetherington, A. M. & Woodward, F. I. The role of stomata in sensing and driving environmental change. *Nature* **424**, 901–908 (2003).
9. Melotto, M., Underwood, W. & He, S. Y. Role of Stomata in Plant Innate Immunity and Foliar Bacterial Diseases. *Annu. Rev. Phytopathol.* **46**, 101–122 (2008).

10. Blatt, M. R., Jezek, M., Lew, V. L. & Hills, A. What can mechanistic models tell us about guard cells, photosynthesis, and water use efficiency? *Trends Plant Sci.* **27**, 166–179 (2022).
11. Kim, T.-H., Böhmer, M., Hu, H., Nishimura, N. & Schroeder, J. I. Guard Cell Signal Transduction Network: Advances in Understanding Abscisic Acid, CO 2 , and Ca 2+ Signaling. *Annu. Rev. Plant Biol.* **61**, 561–591 (2010).
12. Bevacqua, E., Zappa, G., Lehner, F. & Zscheischler, J. Precipitation trends determine future occurrences of compound hot–dry events. *Nat. Clim. Chang.* **12**, 350–355 (2022).
13. Coughlan de Perez, E., Ganapathi, H., Masukwedza, G. I. T., Griffin, T. & Kelder, T. Potential for surprising heat and drought events in wheat-producing regions of USA and China. *npj Clim. Atmos. Sci.* **6**, 56 (2023).
14. Mazdiyasni, O. & AghaKouchak, A. Substantial increase in concurrent droughts and heatwaves in the United States. *Proc. Natl. Acad. Sci.* **112**, 11484–11489 (2015).
15. Ciais, P. *et al.* Europe-wide reduction in primary productivity caused by the heat and drought in 2003. *Nature* **437**, 529–533 (2005).
16. Suzuki, N., Rivero, R. M., Shulaev, V., Blumwald, E. & Mittler, R. Abiotic and biotic stress combinations. *New Phytol.* **203**, 32–43 (2014).
17. Xu, X., Fonseca de Lima, C. F., Vu, L. D. & De Smet, I. When drought meets heat – a plant omics perspective. *Front. Plant Sci.* **14**, (2023).
18. Kholodenko, B. N. & Okada, M. Reengineering protein-phosphorylation switches. *Science (80-.).* **373**, 25–26 (2021).
19. Shindo, Y. *et al.* Conversion of graded phosphorylation into switch-like nuclear translocation via autoregulatory mechanisms in ERK signalling. *Nat. Commun.* **7**, 10485 (2016).
20. Dubois, M. & Inzé, D. Plant growth under suboptimal water conditions: early responses and methods to study them. *J. Exp. Bot.* **71**, 1706–1722 (2020).
21. Sussmilch, F. C., Schultz, J., Hedrich, R. & Roelfsema, M. R. G. Acquiring Control: The Evolution of Stomatal Signalling Pathways. *Trends Plant Sci.* **24**, 342–351 (2019).
22. Hetherington, A. M. Guard Cell Signaling. *Cell* **107**, 711–714 (2001).
23. Roelfsema, M. R. G., Hedrich, R. & Geiger, D. Anion channels: master switches of stress responses. *Trends Plant Sci.* **17**, 221–229 (2012).
24. Hauser, F., Waadt, R. & Schroeder, J. I. Evolution of Abscisic Acid Synthesis and Signaling Mechanisms. *Curr. Biol.* **21**, R346–R355 (2011).
25. Maheshwari, P., Assmann, S. M. & Albert, R. A Guard Cell Abscisic Acid (ABA) Network Model That Captures the Stomatal Resting State. *Front. Physiol.* **11**, (2020).
26. Ueno, K., Kinoshita, T., Inoue, S. I., Emi, T. & Shimazaki, K. I. Biochemical characterization of plasma membrane H+-ATPase activation in guard cell protoplasts of Arabidopsis thaliana in response to blue light. *Plant Cell Physiol.* **46**, 955–963 (2005).
27. Merlot, S. *et al.* Constitutive activation of a plasma membrane H+-ATPase prevents abscisic acid-mediated stomatal closure. *EMBO J.* **26**, 3216–3226 (2007).
28. Toh, S. *et al.* Overexpression of Plasma Membrane H+-ATPase in Guard Cells Enhances Light-Induced Stomatal Opening, Photosynthesis, and Plant Growth in Hybrid Aspen. *Front. Plant Sci.* **12**, (2021).
29. Hayashi, M., Inoue, S., Takahashi, K. & Kinoshita, T. Immunohistochemical Detection of Blue Light-Induced Phosphorylation of the Plasma Membrane H+-ATPase in Stomatal Guard Cells. *Plant Cell Physiol.* **52**, 1238–1248 (2011).
30. Fuglsang, A. T. *et al.* Binding of 14-3-3 Protein to the Plasma Membrane H+-ATPase AHA2 Involves the Three C-terminal Residues Tyr946-Thr-Val and Requires Phosphorylation of Thr947. *J. Biol. Chem.* **274**, 36774–36780 (1999).
31. Svennelid, F. *et al.* Phosphorylation of Thr-948 at the C Terminus of the Plasma

Membrane H + -ATPase Creates a Binding Site for the Regulatory 14-3-3 Protein. *Plant Cell* **11**, 2379–2391 (1999).
32. Falhof, J., Pedersen, J. T., Fuglsang, A. T. & Palmgren, M. Plasma Membrane H + -ATPase Regulation in the Center of Plant Physiology. *Mol. Plant* **9**, 323–337 (2016).
33. Hayashi, Y. *et al.* Phosphorylation of plasma membrane H+-ATPase Thr881 participates in light-induced stomatal opening. *Nat. Commun.* **15**, 1194 (2024).
34. Miao, R., Russinova, E. & Rodriguez, P. L. Tripartite hormonal regulation of plasma membrane H+-ATPase activity. *Trends Plant Sci.* **27**, 588–600 (2022).
35. Kinoshita, T. Blue light activates the plasma membrane H+-ATPase by phosphorylation of the C-terminus in stomatal guard cells. *EMBO J.* **18**, 5548–5558 (1999).
36. Belin, C. *et al.* Identification of Features Regulating OST1 Kinase Activity and OST1 Function in Guard Cells. *Plant Physiol.* **141**, 1316–1327 (2006).
37. Mustilli, A.-C., Merlot, S., Vavasseur, A., Fenzi, F. & Giraudat, J. Arabidopsis OST1 Protein Kinase Mediates the Regulation of Stomatal Aperture by Abscisic Acid and Acts Upstream of Reactive Oxygen Species Production. *Plant Cell* **14**, 3089–3099 (2002).
38. Rizhsky, L. *et al.* When Defense Pathways Collide. The Response of Arabidopsis to a Combination of Drought and Heat Stress. *Plant Physiol.* **134**, 1683–1696 (2004).
39. Sinha, R. *et al.* Differential regulation of flower transpiration during abiotic stress in annual plants. *New Phytol.* **235**, 611–629 (2022).
40. Crawford, A. J., McLachlan, D. H., Hetherington, A. M. & Franklin, K. A. High temperature exposure increases plant cooling capacity. *Curr. Biol.* **22**, R396–R397 (2012).
41. Kostaki, K.-I. I. *et al.* Guard Cells Integrate Light and Temperature Signals to Control Stomatal Aperture. *Plant Physiol.* **182**, 1404–1419 (2020).
42. Gommers, C. Keep Cool and Open Up: Temperature-Induced Stomatal Opening. *Plant Physiol.* **182**, 1188–1189 (2020).
43. Takemiya, A. *et al.* Phosphorylation of BLUS1 kinase by phototropins is a primary step in stomatal opening. *Nat. Commun.* **4**, 2094 (2013).
44. Fuji, S. *et al.* Light-induced stomatal opening requires phosphorylation of the C-terminal autoinhibitory domain of plasma membrane H+-ATPase. *Nat. Commun.* **15**, 1195 (2024).
45. Vu, L. D. *et al.* The membrane-localized protein kinase MAP4K4/TOT3 regulates thermomorphogenesis. *Nat. Commun.* **12**, 2842 (2021).
46. Gupta, A., Rico-Medina, A. & Caño-Delgado, A. I. The physiology of plant responses to drought. *Science (80-.).* **368**, 266–269 (2020).
47. Hõrak, H., Fountain, L., Dunn, J. A., Landymore, J. & Gray, J. E. Leaf temperature responses to ABA and dead bacteria in wheat and Arabidopsis. *Plant Signal. Behav.* **16**, 1899471 (2021).
48. Munemasa, S. *et al.* Mechanisms of abscisic acid-mediated control of stomatal aperture. *Curr. Opin. Plant Biol.* **28**, 154–162 (2015).
49. Urban, J., Ingwers, M., McGuire, M. A. & Teskey, R. O. Stomatal conductance increases with rising temperature. *Plant Signal. Behav.* **12**, e1356534 (2017).
50. Urban, J., Ingwers, M. W., McGuire, M. A. & Teskey, R. O. Increase in leaf temperature opens stomata and decouples net photosynthesis from stomatal conductance in Pinus taeda and Populus deltoides x nigra. *J. Exp. Bot.* **68**, 1757–1767 (2017).
51. Lin, W. *et al.* TMK-based cell-surface auxin signalling activates cell-wall acidification. *Nature* **599**, 278–282 (2021).
52. Kavi Kishor, P. B., Tiozon, R. N., Fernie, A. R. & Sreenivasulu, N. Abscisic acid and its role in the modulation of plant growth, development, and yield stability. *Trends Plant Sci.* **27**, 1283–1295 (2022).

53. Raghavendra, A. S., Gonugunta, V. K., Christmann, A. & Grill, E. ABA perception and signalling. *Trends Plant Sci.* **15**, 395–401 (2010).
54. Takahashi, Y. *et al.* MAP3Kinase-dependent SnRK2-kinase activation is required for abscisic acid signal transduction and rapid osmotic stress response. *Nat. Commun.* **11**, 12 (2020).
55. Waadt, R. *et al.* Identification of Open Stomata1-Interacting Proteins Reveals Interactions with Sucrose Non-fermenting1-Related Protein Kinases2 and with Type 2A Protein Phosphatases That Function in Abscisic Acid Responses. *Plant Physiol.* **169**, 760–779 (2015).
56. Vu, L. D. *et al.* Developmental Plasticity at High Temperature. *Plant Physiol.* **181**, 399–411 (2019).
57. O'sullivan, O. S. *et al.* Thermal limits of leaf metabolism across biomes. *Glob. Chang. Biol.* **23**, 209–223 (2017).
58. Li, L. *et al.* Cell surface and intracellular auxin signalling for H+ fluxes in root growth. *Nature* **599**, 273–277 (2021).
59. Haruta, M., Sabat, G., Stecker, K., Minkoff, B. B. & Sussman, M. R. A Peptide Hormone and Its Receptor Protein Kinase Regulate Plant Cell Expansion. *Science (80-.).* **343**, 408–411 (2014).
60. Merilo, E. *et al.* Abscisic Acid Transport and Homeostasis in the Context of Stomatal Regulation. *Mol. Plant* **8**, 1321–1333 (2015).
61. Schroeder, J. I., Kwak, J. M. & Allen, G. J. Guard cell abscisic acid signalling and engineering drought hardiness in plants. *Nature* **410**, 327–330 (2001).
62. Devireddy, A. R., Arbogast, J. & Mittler, R. Coordinated and rapid whole-plant systemic stomatal responses. *New Phytol.* **225**, 21–25 (2020).
63. Clough, S. J. & Bent, A. F. Floral dip: a simplified method forAgrobacterium-mediated transformation ofArabidopsis thaliana. *Plant J.* **16**, 735–743 (1998).
64. Jinn, T.-L. Using silicon polymer impression technique and scanning electron microscopy to measure stomatal apertures. *BIO-PROTOCOL* **7**, (2017).
65. Huang, Y.-C. *et al.* PECTIN METHYLESTERASE34 Contributes to Heat Tolerance through Its Role in Promoting Stomatal Movement. *Plant Physiol.* **174**, 748–763 (2017).
66. Scarpeci, T., Zanor, M. & Valle, E. Estimation of Stomatal Aperture in Arabidopsis thaliana Using Silicone Rubber Imprints. *BIO-PROTOCOL* **7**, (2017).
67. Hiyama, A. *et al.* Blue light and CO2 signals converge to regulate light-induced stomatal opening. *Nat. Commun.* **8**, 1284 (2017).
68. Wang, P. *et al.* Mapping proteome-wide targets of protein kinases in plant stress responses. *Proc. Natl. Acad. Sci.* **117**, 3270–3280 (2020).
69. Vanhaeren, H. *et al.* UBP12 and UBP13 negatively regulate the activity of the ubiquitin-dependent peptidases DA1, DAR1 and DAR2. *Elife* **9**, (2020).
70. Pizzio, G., Regmi, K. & Gaxiola, R. Rhizosphere Acidification Assay. *BIO-PROTOCOL* **5**, (2015).
71. Pizzio, G. A. *et al.* Arabidopsis Type I Proton-Pumping Pyrophosphatase Expresses Strongly in Phloem, Where It Is Required for Pyrophosphate Metabolism and Photosynthate Partitioning. *Plant Physiol.* **167**, 1541–1553 (2015).
72. Abas, L. *et al.* Intracellular trafficking and proteolysis of the Arabidopsis auxin-efflux facilitator PIN2 are involved in root gravitropism. *Nat. Cell Biol.* **8**, 249–256 (2006).
73. Wang, Y. *et al.* Overexpression of plasma membrane H + -ATPase in guard cells promotes light-induced stomatal opening and enhances plant growth. *Proc. Natl. Acad. Sci.* **111**, 533–538 (2014).
74. Hayashi, Y., Takahashi, K., Inoue, S. I. & Kinoshita, T. Abscisic acid suppresses hypocotyl elongation by dephosphorylating plasma membrane H+-ATPase in

arabidopsis thaliana. *Plant Cell Physiol.* **55**, 845–853 (2014).
75. Grefen, C. & Blatt, M. R. A 2in1 cloning system enables ratiometric bimolecular fluorescence complementation (rBiFC). *Biotechniques* **53**, 311–314 (2012).
76. Mehlhorn, D. G., Wallmeroth, N., Berendzen, K. W. & Grefen, C. 2in1 vectors improve in planta BiFC and FRET analyses. *Methods Mol. Biol.* **1691**, 139–158 (2018).
77. Lu, Q. *et al.* Proteome-wide cellular thermal shift assay reveals unexpected cross-talk between brassinosteroid and auxin signaling. *Proc. Natl. Acad. Sci. U. S. A.* **119**, (2022).
78. Obrdlik, P. *et al.* K + channel interactions detected by a genetic system optimized for systematic studies of membrane protein interactions. *Proc. Natl. Acad. Sci.* **101**, 12242–12247 (2004).
79. Xu, X., Gevaert, K., De Smet, I. & Vu, L. D. Targeted Profiling of Protein Phosphorylation in Plants. in *Methods in Molecular Biology* vol. 2718 167–179 (2023).
80. Tyanova, S. *et al.* The Perseus computational platform for comprehensive analysis of (prote)omics data. *Nat. Methods* **13**, 731–740 (2016).

Figures

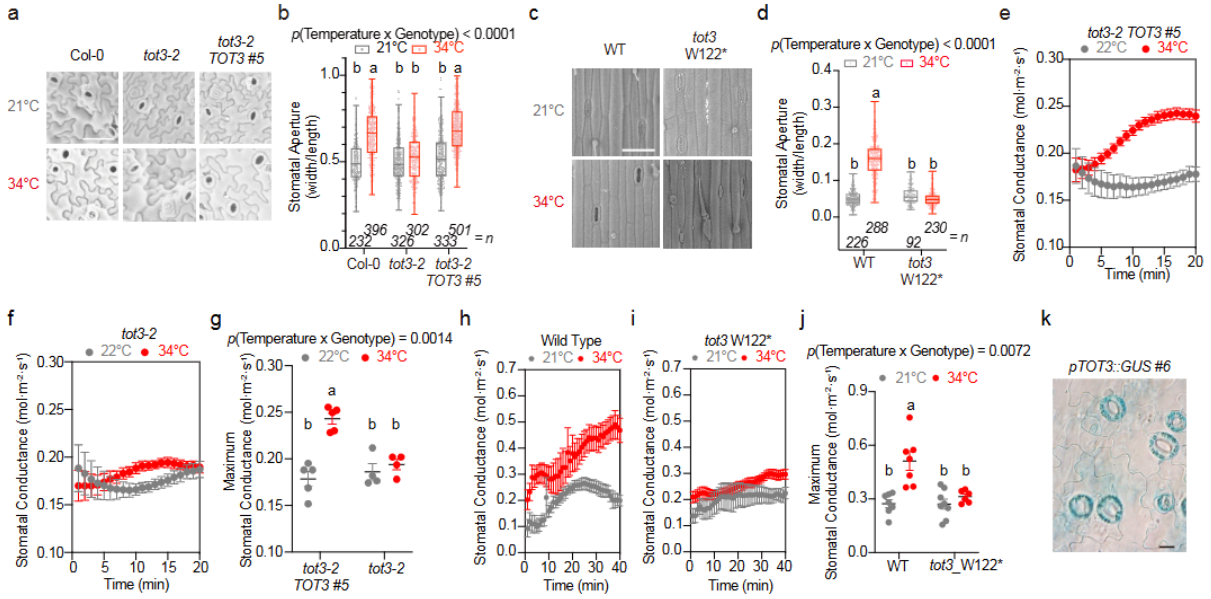

Fig. 1. TOT3 regulates stomatal aperture and conductance under high temperature in dicot and monocot plants. (a-d) Representative scanning electron microscope (SEM) images (a, c), and quantification of stomatal aperture (b, d) of the third leaf epidermis of 3-week-old *Arabidopsis* wild-type Col-0, *tot3-2* mutant and a *tot3-2 pTOT3::GFP:TOT3 #5* (*tot3-2 TOT3*) complementation line grown on agar plates (a-b), and of 3-week-old Cadenza wheat wild-type and *tot3* W122* lines grown in soil (c-d). Box plots (b) and (d) with individual data points represent the distribution of all individual stomata measured, showing the median with Tukey-based whiskers. The whiskers represent the range of the data that is within 1.5 times the interquartile range from the first quartile and third quartile. The values beneath the boxplots (*n*) indicate the number of stomata measured from third leaves from independent *Arabidopsis* Col-0 (12 and 12), *tot3-2* (18 and 18), and *tot3-2 TOT3 #5* (15 and 18), and wheat wild-type (WT) (14 and 11) and *tot3 W122** (9 and 13) plants at 21°C and 34°C, respectively. **(e-j)** Stomatal conductance parameters of *Arabidopsis* (e-g) and wheat (h-j) taken under controlled VPD conditions. Ten-leaf-stage *Arabidopsis* plants of complementation line (*TOT3 tot3-2*) (e) and *tot3-2* mutant (f), and 3-week-old wheat WT (h) and *tot3 W122** (i), grown in soil, were exposed to 21/22°C or 34°C. The experiments were performed at least 4 or 6 times in *Arabidopsis* or wheat, respectively, with independent plants for each line, with similar results. The average value with standard error of the mean is shown in (e-f) and (h-i). The graph with maximum stomatal conductance (dot plot) when environmental condition stability was reached from 15 to 20 min in (g) and 20 to 40 min in (j) includes the median with standard error of the mean. **(k)** Representative β-GLUCURONIDASE (GUS) histochemical staining image of a rosette leaf of a 2-week-old *Arabidopsis* plant expressing *pTOT3::GUS* grown under continuous light at 21°C grown on agar plates. The experiments were repeated three times using three different plants, with similar results. Scale bars = 50 µm (a), 100 µm (c) and 50 µm (k). For all statistical analyses, letters indicate significant differences based on two-way ANOVA and Tukey's test [$p < 0.01$ (b,d) or $p < 0.05$ (e-j)] between 21°C and 34°C. The *p*-value for the interaction (temperature x genotype) is shown at the top.

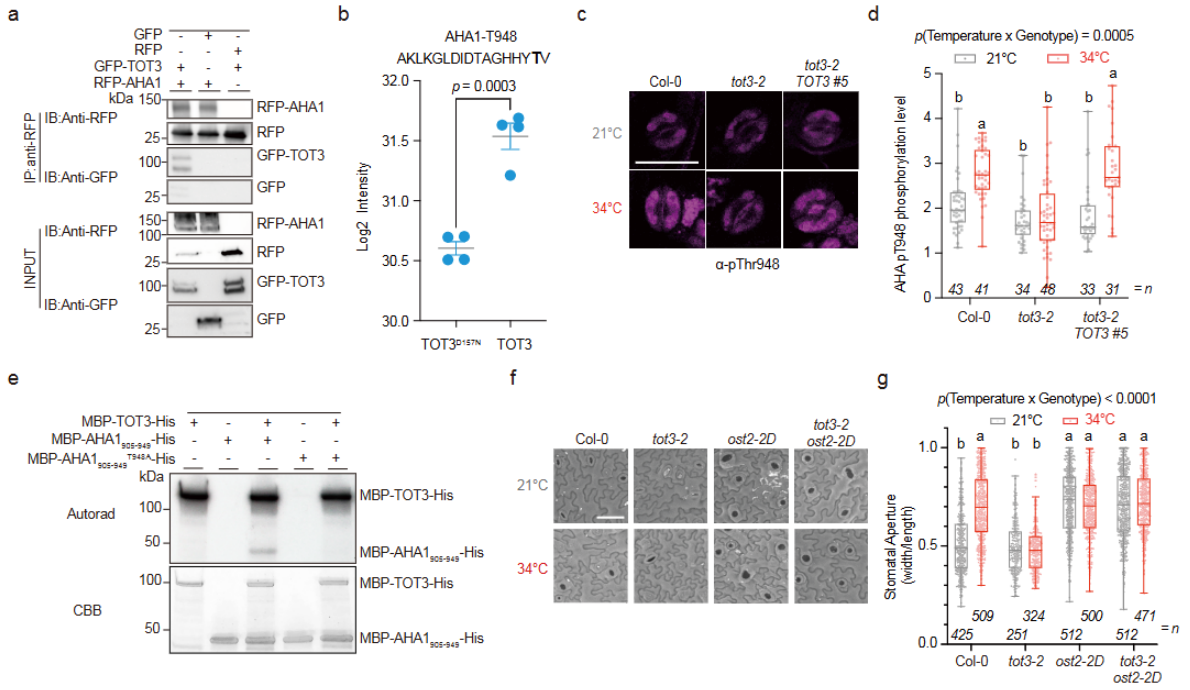

Fig. 2. TOT3 phosphorylates AHA1 to regulate stomatal aperture under high temperature. (a) Co-immunoprecipitation of GFP-TOT3 and RFP-AHA1 following transient expression in *Nicotiana benthamiana* leaves. After IP, truncated RFP from RFP-AHA1 was possibly detected by anti-RFP. The experiment was repeated independently three times, with similar results. **(b)** Log2 phosphorylation intensity of an AHA1 phosphopeptide that contains T948 (in bold) as detected through mass spectrometry from AHA1 co-expressed with wild-type TOT3 or kinase-dead TOT3^{D157N} in *N. benthamiana* leaves. The scatter plots show the mean of four biological replicates, with the standard error of the mean. The *p*-value was calculated by unpaired, two-tailed t-test. **(c-d)** Representative fluorescence images (c) and intensity quantification (d) of immunohistochemical detection of H^+-ATPase penultimate threonine phosphorylation by an antibody against the penultimate threonine in guard cells of Col-0 wild-type, *tot3-2*, and *tot3-2 pTOT3::GFP:TOT3 #5* (*tot3-2 TOT3 #5*), exposed to 21°C or 34°C for 15 minutes in stomatal buffer. The value under the bars indicates the number of stomata measured (*n*) from a mixture of several rosette leaves. **(e)** *In vitro* phosphorylation assay autoradiogram (with [γ-32P]ATP) of recombinant TOT3 incubated with the C-terminal fragment of AHA1. The lower gel shows Coomassie brilliant blue (CBB) staining as the loading control. The different phosphorylation of kinase and substrates in the autoradiogram picture is likely due to several residues of full-length TOT3 being auto-phosphorylated and because only one residue of AHA1 could be phosphorylated by TOT3. The experiment was repeated independently three times, with similar results. **(f-g)** Representative SEM images of the third leaf epidermis of 3-week-old *Arabidopsis* Col-0, *tot3-2*, *ost2-2D* and *tot3-2 ost2-2D* (f) and quantification of stomatal aperture (g) on agar plates. The value under the bars (*n*) indicates the number of stomata measured from individual third leaves from independent *Arabidopsis* Col-0 (22 and 14), *tot3-2* (18 and 13), *ost2-2D* (14 and 14) and *tot3-2 ost2-2D* (14 and 14*)* plants at 21°C and 34°C, respectively. For d and g, box plots with individual data points represent the distribution of all individual stomata measured, showing the median with Tukey-based whiskers. The whiskers represent the range of the data that is within 1.5 times the interquartile range from the first quartile and third quartile. Letters indicate significant differences based on two-way ANOVA and Tukey's test ($p < 0.01$) between 21°C and 34°C. The interaction (temperature x genotype) *p*-value is shown at the top. Scale bars = 25 µm (c), and 50 µm (f).

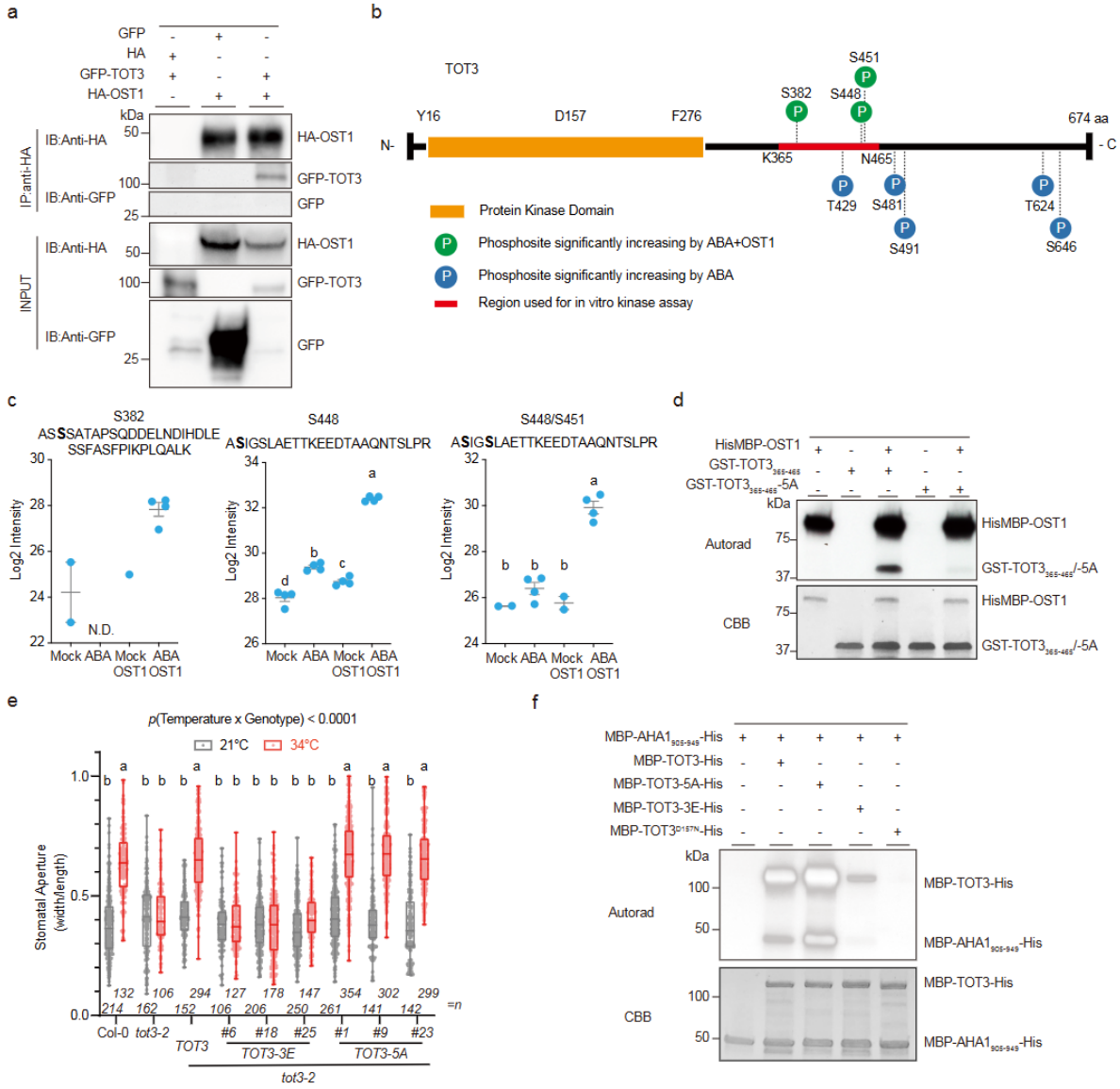

Fig. 3. OST1-mediated TOT3 phosphorylation regulates stomatal aperture under high temperature. (a) Co-IP of GFP-TOT3 and HA-OST1 transiently expressed in *Nicotiana benthamiana* leaves. The experiment was repeated independently three times with similar results. **(b)** Schematic diagram of the TOT3 protein with relevant phosphosites mediated by OST1 and/or ABA indicated. **(c)** Log2 phosphorylation intensity of TOT3 phosphopeptides mediated by OST1 and ABA, that contain S382, S448 and S451 (in bold), as detected through mass spectrometry from TOT3 co-expressed with/without OST1 and/or ABA in *Nicotiana benthamiana* leaves. The graph shows the mean of four biological replicates, with a standard error of the mean. Letters indicate significant differences based on one-way ANOVA and Tukey's test ($p < 0.01$). N.D. = not detected. **(d)** *In vitro* kinase assay autoradiogram ([γ-32P]ATP) with recombinant OST1 and a TOT3 fragment (365-465) comprising the phosphosites indicated in B-C. The lower gel shows CBB staining as the loading control. The experiment was repeated independently four times with similar results. The different phosphorylation intensity of OST1 and the TOT3 fragment in the autoradiogram picture is likely due to many auto-phosphorylated residues of full-length OST1 compared to only three TOT3 residues that could be phosphorylated by OST1. **(e)** Stomatal aperture of *tot3-2* mutant and *tot3-2* expressing *pTOT3::GFP:TOT3 #5* (*tot3-2 TOT3 #5*), *pTOT3::GFP:TOT3-3E #6*, *#18* and *#25* (*tot3-2 TOT3-3E #6*, *#18* and *#25*), or *pTOT3::GFP:TOT3-5A #1*, *#9* and *#23* (*tot3-2 TOT3-5A #1*, *#9* and *#23*) on agar plates. Box plots with individual data points represent

the distribution of all individual stomata measured, showing the median with Tukey-based whiskers. The whiskers represent the range of the data that is within 1.5 times the interquartile range from the first quartile and third quartile. Letters indicate significant differences based on two-way ANOVA and Tukey's test ($p < 0.01$) between 21 and 34°C. The *p*-value for the interaction (temperature x genotype) is shown at the top. The values beneath the boxplots (*n*) represent the number of stomata measured from third leaves from independent *Arabidopsis* Col-0 (6 and 8), *tot3*-2 (5 and 6), *tot3-2 TOT3 #5* (8 and 5), *tot3-2 TOT3-3E #6* (6 and 6), *tot3-2 TOT3-3E #18* (8 and 8), *tot3-2 TOT3-3E #18* (6 and 9), *tot3-2 TOT3-5A #1* (9 and 7), *tot3-2 TOT3-5A #9* (9 and 6), and *tot3-2 TOT3-5A #23* (8 and 6) plants at 21°C and 34°C, respectively. **(f)** *In vitro* kinase assay autoradiogram ([γ-32P]ATP) of the C-terminal fragment of AHA1 (905-949) and TOT3, or TOT3-5A, or TOT3-3E, or kinase dead $TOT3^{D157N}$. The lower gel shows CBB staining as the loading control. The experiment was repeated independently three times with similar results.

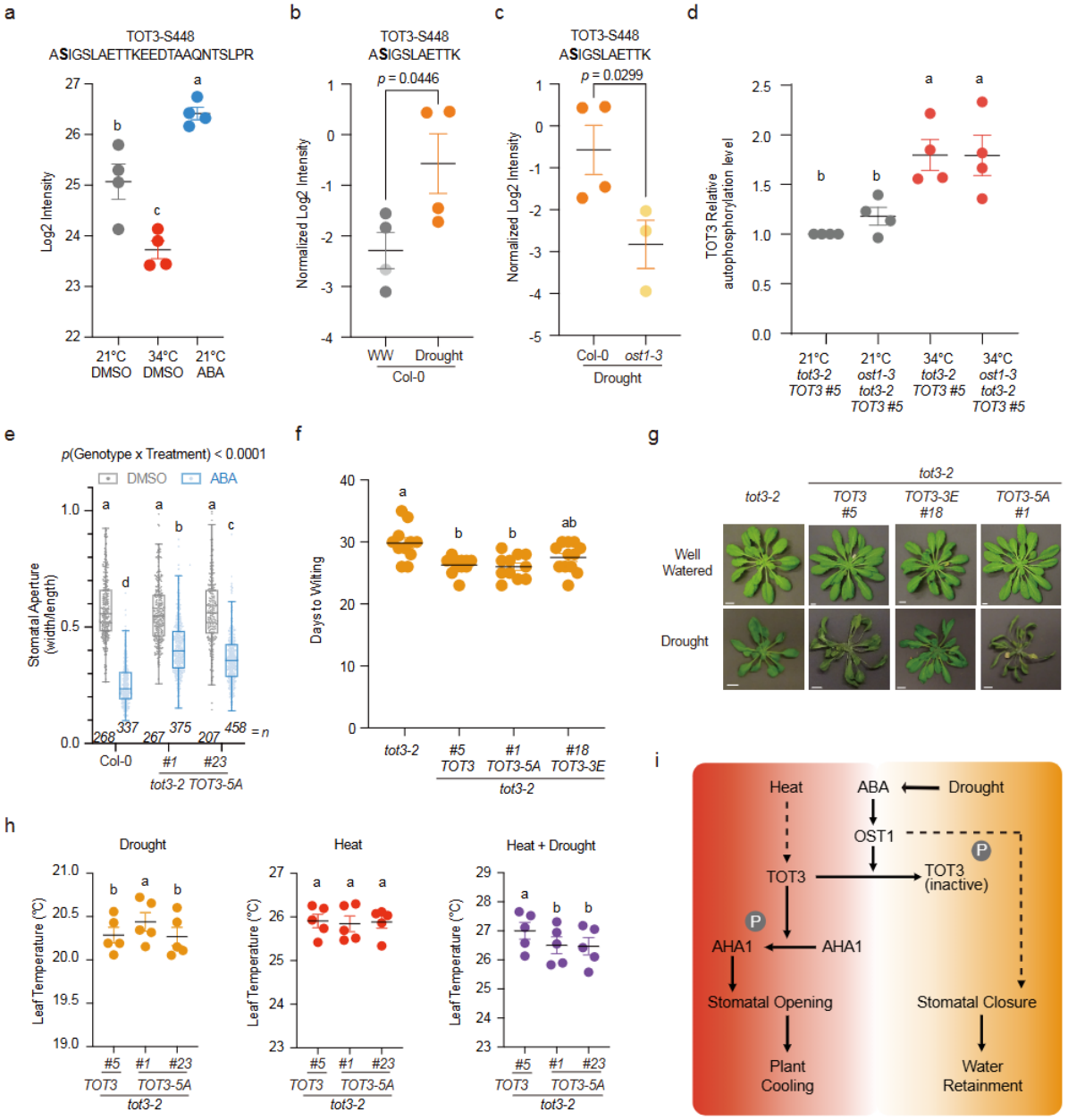

Fig. 4. OST1-mediated phosphorylation of TOT3 affects drought tolerance and leaf temperature under drought. (a) Log2 intensity of a TOT3 phosphopeptide containing S448 (in bold) in shoots of 2-week-old *tot3-2 pTOT3::GFP:TOT3 #5* plants treated with DMSO or 50 µM ABA at 21°C or 34 °C in liquid half-strength MS for one hour. Scatter plots show individual Log2 values from 4 independent plants, with standard error of the mean. Letters indicate significant differences based on the one-way ANOVA ($p < 0.05$). (**b-c**) Normalized Log2 intensity of a TOT3 phosphopeptide containing S448 (in bold) under well-watered (WW) or progressive drought conditions in Col-0 wild-type under well-watered or drought conditions (b), and under drought conditions in Col-0 or *ost1-3* (c) in soil. Each dot represents a biological replicate. Data are presented as mean values with the standard error of the mean (SEM) and *p*-value calculated by an unpaired two-tailed t-test is indicated. The pale grey- and orange-coloured dots indicate imputed values (phosphopeptide not detected by mass spectrometry). **(d)** Relative TOT3 autophosphorylation level from *in vitro* phosphorylation assays using TOT3 pulled down from shoots of two two-week-old plants of *tot3-2 pTOT3::GFP:TOT3 #5 (tot3-2 TOT3 #5)* or *ost1-3 tot3-2 pTOT3::GFP:TOT3 #5 (ost1-3 tot3-2 TOT3 #5)* grown on agar plates

exposed to 21°C or 34°C for 2 h. Scatter plots show the mean of individual values from five biological replicates. Letters indicate significant differences based on one-way ANOVA and Tukey's test ($p < 0.05$) for each indicated condition. **(e)** The stomatal aperture of Col-0 wild-type, independent *tot3-2 pTOT3::GFP:TOT3-5A (tot3-2 TOT3-5A #1* and *#23)* lines on agar plates treated with 10 µM ABA or DMSO for 2 hours. Box plots with individual data points represent the distribution of all individual stomata measured, showing the median with Tukey-based whiskers. The whiskers represent the range of the data that is within 1.5 times the interquartile range from the first quartile and third quartile. Letters indicate significant differences based on two-way ANOVA and Tukey's test ($p < 0.01$) between Mock and ABA treatment. The value under the bars (*n*) indicates the number of stomata measured from independent third leaves from independent *Arabidopsis* Col-0 (12 and 19), *tot3-2 TOT3-5A #1* (12 and 19), *tot3-2 TOT3-5A #23* (12 and 22) plants under DMSO and ABA treatment, respectively. **(f)** Days to wilting counted after the start of withholding water of indicated soil-grown lines of *tot3-2* mutant and *tot3-2* expressing *pTOT3::GFP:TOT3 #5 (tot3-2 TOT3)*, *pTOT3::GFP:TOT3-5A #1* (*tot3-2 TOT3-5A*), or *pTOT3::GFP:TOT3-3E #18* (*tot3-2 TOT3-3E*) at 21°C. Letters indicate significant differences based on one-way ANOVA ($p < 0.01$). The scatter plots with individual data points show the distribution of independent plants for 11 biological replicates of *tot3-2*, *tot3-2 TOT3 #5*, and *tot3-2 TOT3-5A #1*, and 12 biological replicates of *tot3-2 TOT3-3E #18*, with the median with Tukey-based whiskers. Letters indicate significant differences based on one-way ANOVA and Tukey's test ($p < 0.05$) among genotypes. **(g)** Representative images of rosette-stage soil-grown plants of *tot3-2* mutant and *tot3-2* expressing *pTOT3::GFP:TOT3 #5 (tot3-2 TOT3 #5)*, *pTOT3::GFP:TOT3-5A #1* (*tot3-2 TOT3-5A #1*), or *pTOT3::GFP:TOT3-3E #18* (*tot3-2 TOT3-3E #18*), subjected to 3 weeks of well-watering (top row) or progressive drought conditions (lower row) at 21°C, initiated when the plants were 3 weeks old. Scale bar = 1 cm. **(h)** Leaf temperature of soil-grown *tot3-2 pTOT3::GFP:TOT3 #5 (tot3-2 TOT3 #5)* and *tot3-2 pTOT3::GFP:TOT3-5A (tot3-2 TOT3-5A #1* and *#23)* under progressive drought (21°C), high temperature (34°C) or combined drought with high temperature (34°C) conditions. The graph shows the mean with SEM (line) of the leaf temperature for 5 consecutive days with Tukey-based whiskers. Each dot on the graph represents the average leaf temperature across all time points for the following replicates on a single day under drought (5, 8, and 6), high temperature (3, 4, and 3), and combined drought and high temperature (4, 3, and 3) for *tot3-2 TOT3 #5*, *tot3-2 TOT3-5A #1* and *tot3-2 TOT3-5A #23*, respectively. Letters indicate significant differences based on one-way ANOVA ($p < 0.01$). **(i)** Proposed model of AHA1-OST1-TOT3 module-regulated stomatal aperture modulation under high temperature and/or drought stress.